

Entropic Wetting and the Free Isotropic–Nematic Interface of Hard Colloidal Platelets

Hendrik Reich,[†] Marjolein Dijkstra,[‡] René van Roij,[§] and Matthias Schmidt^{*,†,||}

Institut für Theoretische Physik II, Heinrich-Heine-Universität Düsseldorf, Universitätsstrasse 1, D-40225 Düsseldorf, Germany, Debye Institute, Soft Condensed Matter, Utrecht University, Princetonplein 5, 3584 CC Utrecht, The Netherlands, Institute for Theoretical Physics, Utrecht University, Leuvenlaan 4, 3584 CE Utrecht, The Netherlands, and H. H. Wills Physics Laboratory, University of Bristol, Royal Fort, Tyndall Avenue, Bristol BS8 1TL, United Kingdom

Received: December 22, 2006; In Final Form: March 5, 2007

We study bulk and interfacial properties of a model suspension of hard colloidal platelets with continuous orientations and vanishing thickness using both density functional theory, based on either a second virial approach or fundamental measure theory (FMT), and Monte Carlo (MC) simulations. We calculate the bulk equation of state, bulk isotropic–nematic (IN) coexistence, and properties of the (planar) free IN interface and of adsorption at a planar hard wall, where we find complete wetting of the nematic phase at the isotropic–wall interface upon approaching bulk IN coexistence. We investigate in detail the asymptotic decay of correlations at large distances. In all cases, the results from FMT and MC agree quantitatively. Our findings are of direct relevance to understanding interfacial properties of dispersions of colloidal platelets.

I. Introduction

Dispersions of nonspherical colloidal particles are model systems to study a variety of phenomena in condensed matter, including fluid phase separation, liquid crystalline ordering, and the influence of magnetic, electric, or gravitational fields on macroscopic properties. The bulk phase behavior of nonspherical colloids is considerably more complex than that of spherical particles due to the stability of partially ordered (liquid crystalline) phases with properties between those of liquids and those of crystals. One particularly important example is the phase transition from an isotropic (I) fluid to an orientationally ordered nematic (N) fluid. The nematic phase is characterized by macroscopic orientational order, such that the particles align preferentially along a common nematic director; the spatial distribution of position coordinates remains homogeneous. The IN transition was first observed experimentally in suspensions of (rodlike) tobacco mosaic virus particles,^{1,2} and its first theoretical description was given by Onsager.³ This famous derivation of macroscopic ordering from anisotropic particle shapes constitutes a paradigm for understanding the competition between position and orientation degrees of freedom that maximizes the overall entropy of the system. Onsager's theory can be viewed as a truncation of the Taylor expansion of the Helmholtz excess free energy functional at second order in density and becomes exact, due to a scaling argument, in the limit of thin rods at high concentration. However, such a scaling does not hold in the case of (vanishingly) thin hard platelets; when applied to this system, the theory is known to predict the bulk isotropic–nematic (IN) transition correctly to be of first order but to overestimate the transition densities and value of the nematic order parameter at coexistence quite severely as compared to simulation results.^{4,5} The peculiar features of the

bulk IN transition of hard platelets are the very small density jump at coexistence and the very low value of the nematic order parameter, $S \sim 0.5$, in the coexisting nematic phase.

During recent years, considerable experimental, simulation, and theoretical work has been devoted to gaining understanding of the behavior of platelet dispersions. A well-established experimental model system is gibbsite platelets dispersed in toluene, for which the existence of the IN transition in a colloidal platelet system was for the first time observed with polarization microscopy.⁷ In the same system the nematic–columnar phase transition,⁸ the hexagonal–columnar liquid crystal phase,⁹ and gelation and nematic ordering¹⁰ were investigated subsequently. Furthermore, the influence of external potentials was considered, e.g., that of gravity^{11,12} and of electric¹³ and magnetic fields.¹⁴ Also, platelike clay particles^{15,16} and mixtures of colloidal platelets and polymers^{17,18} have received considerable attention. Theoretical investigations were devoted to the influence of gravity on phase behavior¹⁹ and the phenomenon of nematic density inversion.²⁰ An interaction site model for lamellar colloids was investigated.²¹ The phase diagram of a mixture of hard colloidal spheres and disks was calculated using a free volume approach,²² and the free IN interface in fluids of charged platelike colloids was investigated using the Zwanzig model with discrete orientations.²³ Ref 24 is devoted to the effects caused by polydispersity in a mixture of rods and platelets. A model fluid of hard platelike particles has also been used to describe the structure factor of macromolecular solutions of stilbenoid dendrimers.⁶

The presence of a substrate commonly leads to rich phenomenology of surface phase behavior. The smooth hard planar wall is a basic model for a substrate which despite its simplicity induces intriguing phenomena—and has accordingly attracted interest for a variety of hard core models. As energy is irrelevant in such systems, one refers to “entropic wetting”,²⁵ and examples include ordering of rods near a hard wall,²⁶ the uniaxial–biaxial transition of hard rods,^{27–29} wetting and layering transitions for model colloid–polymer mixtures,^{30–37} and wetting of hard

* Corresponding author.

[†] Heinrich-Heine-Universität Düsseldorf.

[‡] Debye Institute, Soft Condensed Matter, Utrecht University.

[§] Institute for Theoretical Physics, Utrecht University.

^{||} University of Bristol.

spheres in a planar hard slit.³⁸ Also, the entropic torque acting on a single hard rod in a solvent of hard spheres close to the wall was investigated.³⁹ The isotropic phase of platelets in contact with a wall has been considered in ref 40 using Onsager theory, and results were compared to those for a hard rod fluid. For the Zwanzig model of platelets,⁴¹ wetting and capillary effects were investigated,⁴² as well as bulk and interfacial properties of binary mixtures.⁴³

Here, we consider vanishingly thin circular hard platelets with continuous orientations addressing the bulk equation of state, the densities of the bulk isotropic–nematic (IN) coexistence, density profiles, and the interface tension of the (planar) free IN interface, as well as the wetting properties when the system is exposed to a planar hard wall. We use Monte Carlo (MC) computer simulations, Onsager theory, and a recently proposed fundamental measure theory (FMT) density functional.⁴⁴ The latter includes contributions to the free energy that are of third order in density and gives values of the coexistence densities and order parameter at the IN transition in good agreement with simulation results. We investigate in detail the results from the respective approaches for the asymptotic decay of density profiles at large distances from a wall.^{45–49} A short account of this work has been published as part of ref 50.

This paper is organized as follows. In section II, we describe the model interactions. Section III gives an overview of density functional theory (DFT) and introduces both the Onsager and the FMT approximations. We present results in section IV for the bulk properties, the IN transition, the free IN interface, and wetting at a hard wall and conclude in section V.

II. Model

Consider a fluid of infinitely thin hard circular platelets of radius R . The platelets interact with a hard core pair potential $\phi(\mathbf{r}, \boldsymbol{\omega}, \boldsymbol{\omega}')$ that depends on the center-to-center distance \mathbf{r} between both platelets and on both orientations, and $\boldsymbol{\omega}$ and $\boldsymbol{\omega}'$, taken to be unit vectors perpendicular to the plane of the particle. The value of $\phi(\mathbf{r}, \boldsymbol{\omega}, \boldsymbol{\omega}')$ is infinite provided that the two particles overlap and vanishes otherwise.

In addition, the system is confined by a planar smooth hard wall, which we take to be perpendicular to the z -direction and to be located at $z = 0$, such that only the halfspace $z > 0$ is accessible to the particles. Hence, the interaction between the hard planar wall and a platelet is described by an external potential,

$$V_{\text{ext}}(z, \theta) = \begin{cases} \infty & \text{if } z < R \sin \theta \\ 0 & \text{otherwise} \end{cases} \quad (1)$$

where θ is the angle between the z -direction (normal to the wall) and the particle orientation $\boldsymbol{\omega}$ (normal to the platelet), which we can choose to be in the range $0 < \theta < \pi/2$ due to the inflection symmetry, $\boldsymbol{\omega} \rightarrow -\boldsymbol{\omega}$, of the particles. See Figure 1a for an illustration of the model.

The one-body density distribution of the platelets is denoted by $\rho(\mathbf{r}, \boldsymbol{\omega})$, where \mathbf{r} is the position coordinate of the particle center. As a bulk parameter, we use the scaled density ρR^3 ; the normalization is chosen such that $\rho = \int d\mathbf{r} d\boldsymbol{\omega} \rho(\mathbf{r}, \boldsymbol{\omega}) / (4\pi V)$, where V is the system volume. As we do not expect biaxiality to occur, we can assume invariance with respect to rotations around the z -axis, as well as translational invariance in the x - and y -directions. The remaining relevant angle θ is that between the orientation $\boldsymbol{\omega}$ and the z -axis; see Figure 1a. It follows that the (number) density distribution $\rho(\mathbf{r}, \boldsymbol{\omega}) = \rho(z, \theta)$.

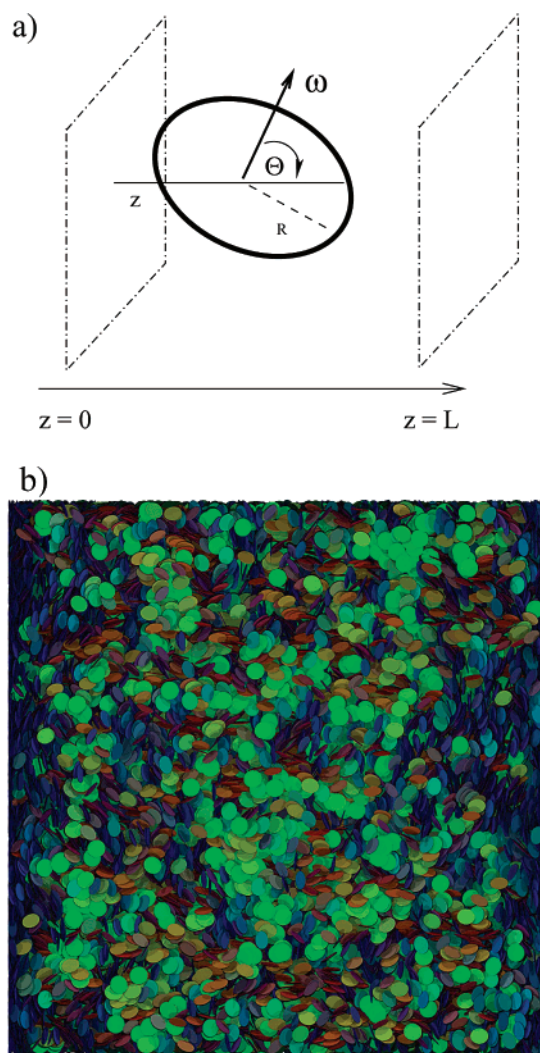


Figure 1. (a) Model of hard platelets with radius R and vanishing thickness at a planar hard wall. The angle between the z -direction, perpendicular to the wall, and the platelet orientation $\boldsymbol{\omega}$ is denoted by θ . For convenience, we also consider a second parallel wall at a distance L . (b) Snapshot from MC simulations using 110 000 particles at a (bulk) density of $\rho R^3 = 0.455$. The system possesses periodic boundary conditions in the x - and y -directions. Particles are colored according to their orientation.

III. Density Functional Theory

A. Overview. In DFT, the grand potential is expressed as a functional of the one-body density distribution,⁵¹

$$\tilde{\Omega}([\rho], \mu) = F_{\text{id}}[\rho] + F_{\text{exc}}[\rho] + \int d\mathbf{r} \int \frac{d\boldsymbol{\omega}}{4\pi} \rho(\mathbf{r}, \boldsymbol{\omega}) (V_{\text{ext}}(\mathbf{r}, \boldsymbol{\omega}) - \mu) \quad (2)$$

where $F_{\text{exc}}[\rho]$ is the excess (over ideal gas) contribution to the total (Helmholtz) free energy functional that arises from interparticle interactions, $V_{\text{ext}}(\mathbf{r}, \boldsymbol{\omega})$ is an external potential acting on the particles, μ is the chemical potential, and the ideal gas (Helmholtz) free energy functional for uniaxial rotators is given by

$$F_{\text{id}}[\rho] = k_{\text{B}} T \int d\mathbf{r} \int \frac{d\boldsymbol{\omega}}{4\pi} \rho(\mathbf{r}, \boldsymbol{\omega}) (\ln(\rho(\mathbf{r}, \boldsymbol{\omega}) \Lambda^3) - 1) \quad (3)$$

where k_{B} is Boltzmann's constant, T is the absolute temperature, and Λ is the (irrelevant) thermal wavelength for which we choose $\Lambda = R$; the dependence on volume V and temperature

has been suppressed in the notation. In the following, we use the scaled chemical potential $\mu^* = \beta\mu$ with $\beta = 1/k_B T$.

For any given external potential $V_{\text{ext}}(\mathbf{r}, \boldsymbol{\omega})$, minimizing the grand potential with respect to the one-body density distribution $\rho(\mathbf{r}, \boldsymbol{\omega})$ gives the equilibrium density profile,

$$\frac{\delta\tilde{\Omega}[\rho]}{\delta\rho(\mathbf{r}, \boldsymbol{\omega})} = 0 \quad (4)$$

which can be rewritten, using eq 2, as an Euler–Lagrange equation

$$k_B T \ln(\rho(\mathbf{r}, \boldsymbol{\omega})\Lambda^3) - k_B T c_1([\rho], \mathbf{r}, \boldsymbol{\omega}) + V_{\text{ext}}(\mathbf{r}, \boldsymbol{\omega}) = \mu \quad (5)$$

where $c_1([\rho], \mathbf{r}, \boldsymbol{\omega}) = -(k_B T)^{-1} \delta F_{\text{exc}}[\rho] / \delta\rho(\mathbf{r}, \boldsymbol{\omega})$ is the one-body direct correlation functional. One systematic way to write down the excess free energy functional is to expand it in a virial series,

$$\begin{aligned} \beta F_{\text{exc}}[\rho] = & -\frac{1}{2} \int d\mathbf{r} \int \frac{d\boldsymbol{\omega}}{4\pi} \int d\mathbf{r}' \int \frac{d\boldsymbol{\omega}'}{4\pi} \rho(\mathbf{r}, \boldsymbol{\omega}) \rho(\mathbf{r}', \boldsymbol{\omega}') f(\mathbf{r} - \mathbf{r}', \boldsymbol{\omega}, \boldsymbol{\omega}') \\ & -\frac{1}{6} \int d\mathbf{r} \int \frac{d\boldsymbol{\omega}}{4\pi} \int d\mathbf{r}' \int \frac{d\boldsymbol{\omega}'}{4\pi} \int d\mathbf{r}'' \int \frac{d\boldsymbol{\omega}''}{4\pi} \\ & \rho(\mathbf{r}, \boldsymbol{\omega}) \rho(\mathbf{r}', \boldsymbol{\omega}') \rho(\mathbf{r}'', \boldsymbol{\omega}'') \times \\ & f(\mathbf{r} - \mathbf{r}', \boldsymbol{\omega}, \boldsymbol{\omega}') f(\mathbf{r} - \mathbf{r}'', \boldsymbol{\omega}, \boldsymbol{\omega}'') f(\mathbf{r}' - \mathbf{r}'', \boldsymbol{\omega}', \boldsymbol{\omega}'') + O(\rho^4) \end{aligned} \quad (6)$$

where $f(\mathbf{r}, \boldsymbol{\omega}, \boldsymbol{\omega}') = \exp(-\beta\phi(\mathbf{r}, \boldsymbol{\omega}, \boldsymbol{\omega}')) - 1$ is the Mayer function that for hard bodies is -1 if the two particles overlap and vanishes otherwise. In practice, one has to resort to approximations to $F_{\text{exc}}[\rho]$ and Onsager's theory relies on truncating eq 6 after the *second order* in density. This is known to be a good approximation for thin rods; we will investigate in detail how it fares for platelets below.

Several approximations of $F_{\text{exc}}[\rho]$ for nonspherical (convex) hard bodies have been proposed: ref 52 gives an FMT for parallel hard cubes; refs 53 and 54 investigate the properties of the Zwanzig model; ref 55 is devoted to the role of three-body correlations in a system of hard rectangles. In ref 56, an interpolation between the Rosenfeld functional⁵⁷ for hard spheres and the Onsager functional for elongated rods was proposed. Our present investigation relies on the theory of ref 44 for a ternary mixture of hard spheres, needles, and platelets with continuous orientations. For completeness, but also to disentangle the pure platelet case from the full ternary mixture, we summarize the main features of the FMT hard platelet functional briefly in the following.

B. Fundamental Measure Theory. The fundamental measure theory (FMT) was built originally for additive hard sphere mixtures.⁵⁷ The extension to arbitrarily shaped hard convex bodies, proposed in refs 58 and 59, yields the correct second virial coefficients in the isotropic phase but only an approximation for the Mayer bond(s), such that even the lowest (second) order term in the virial expansion (6) of the excess free energy functional is not correct. This is not sufficient to describe, e.g., nematic ordering (see, e.g., ref 56 for a discussion). The theory of ref 44 remedies this deficiency for the case of hard platelets of vanishing thickness. Hence, it possesses the correct contribution of second order in density and also features a term of third order in density. Higher order terms are absent, which is intimately connected to the scaled-particle roots of the approach and can in particular be traced back to the vanishing volume of the particles, which leads to a vanishing packing fraction. The

third-order term is different from the exact third virial contribution (as given in eq 6). It is nonvanishing (and constant) for cases with common triple intersection of the three particles involved. Global prefactors are used to compensate for the “lost cases”^{60,61} in order to yield reasonable values for the third virial coefficients (of the ternary mixture). For a more detailed discussion, we refer the reader to ref 44.

The excess free energy functional is expressed as an integral over space and (in the present case of platelets) twice over director space,

$$\beta F_{\text{exc}}[\rho] = \int d\mathbf{r} \int \frac{d\boldsymbol{\omega}}{4\pi} \int \frac{d\boldsymbol{\omega}'}{4\pi} \Phi(\{n_i^v\}) \quad (7)$$

where the (reduced) free energy density, Φ , is a function of a set of weighted densities, $\{n_i^v\}$, where v and i label the type of weighted density (detailed below); the arguments \mathbf{r} , $\boldsymbol{\omega}$, and $\boldsymbol{\omega}'$ of the weighted densities have been omitted in the notation. For pure platelets, the free energy density is

$$\Phi(\{n_i^v\}) = n_1^{\text{DD}}(\mathbf{r}, \boldsymbol{\omega}) n_2^{\text{D}}(\mathbf{r}, \boldsymbol{\omega}) + \frac{1}{24\pi} n_2^{\text{D}}(\mathbf{r}, \boldsymbol{\omega}) n_2^{\text{DDD}}(\mathbf{r}; \boldsymbol{\omega}; \boldsymbol{\omega}') n_2^{\text{D}}(\mathbf{r}, \boldsymbol{\omega}') \quad (8)$$

where the first term on the right-hand side (rhs) when combined with eq 7 recovers the exact second virial contribution to $F_{\text{exc}}[\rho]$ (see section III.C of ref 44 for an explicit derivation). The weighted densities are related to the bare one-body density, $\rho(\mathbf{r}, \boldsymbol{\omega})$, via

$$n_2^{\text{D}}(\mathbf{r}, \boldsymbol{\omega}) = w_2^{\text{D}}(\mathbf{r}, \boldsymbol{\omega}) * \rho(\mathbf{r}, \boldsymbol{\omega}) \quad (9)$$

$$n_1^{\text{DD}}(\mathbf{r}, \boldsymbol{\omega}) = \int \frac{d\boldsymbol{\omega}'}{4\pi} w_1^{\text{DD}}(\mathbf{r}, \boldsymbol{\omega}'; \boldsymbol{\omega}) * \rho(\mathbf{r}, \boldsymbol{\omega}') \quad (10)$$

$$n_2^{\text{DDD}}(\mathbf{r}; \boldsymbol{\omega}; \boldsymbol{\omega}') = \int \frac{d\boldsymbol{\omega}''}{4\pi} w_2^{\text{DDD}}(\mathbf{r}, \boldsymbol{\omega}''; \boldsymbol{\omega}; \boldsymbol{\omega}') * \rho(\mathbf{r}, \boldsymbol{\omega}'') \quad (11)$$

where $*$ denotes the three-dimensional convolution and the weight functions are given by

$$w_1^{\text{D}}(\mathbf{r}, \boldsymbol{\omega}) = \delta(R - |\mathbf{r}|) \delta(\mathbf{r} \cdot \boldsymbol{\omega}) / 8 \quad (12)$$

$$w_2^{\text{D}}(\mathbf{r}, \boldsymbol{\omega}) = 2\Theta(R - |\mathbf{r}|) \delta(\mathbf{r} \cdot \boldsymbol{\omega}) \quad (13)$$

$$w_1^{\text{DD}}(\mathbf{r}, \boldsymbol{\omega}; \boldsymbol{\omega}') = \frac{2}{R} |\boldsymbol{\omega} \cdot (\boldsymbol{\omega}' \times \mathbf{r})| w_1^{\text{D}}(\mathbf{r}, \boldsymbol{\omega}) \quad (14)$$

$$w_2^{\text{DDD}}(\mathbf{r}, \boldsymbol{\omega}; \boldsymbol{\omega}'; \boldsymbol{\omega}'') = \frac{8}{\pi} |\boldsymbol{\omega} \cdot (\boldsymbol{\omega}' \times \boldsymbol{\omega}'')| w_2^{\text{D}}(\mathbf{r}, \boldsymbol{\omega}) \quad (15)$$

where $\Theta(\cdot)$ is the unit step (Heaviside) function and $\delta(\cdot)$ is the Dirac distribution. We have kept the notation of ref 44 where the upper index D refers to the species (disks) and its number of appearances indicates the number of particle orientations that appear in the weight function, eqs 12–15. The lower index i indicates whether the weight function is characteristic of the rim ($i = 1$) or of the surface ($i = 2$) of the particles.

C. Numerical Procedure. To obtain the weight functions and hence the weighted densities in planar geometry, we integrate over the in-plane coordinates x and y in eqs 9–11, assuming azimuthal symmetry such that the density distribution only depends on z and θ ; See section VII of ref 44 for explicit results. Our numerical implementation of eq 5 uses free minimization, i.e., no *a priori* form of $\rho(z, \theta)$ is assumed. For practical reasons, we add a second hard wall, such that the walls are located at $z = 0$ and $z = L$, with typically $L/R = 51$, which

we find to be large enough to prevent significant capillary effects. An equidistant grid in the z direction with 20 grid points per particle radius R is used. The angle θ is discretized on a nonequidistant grid with 20 grid points in the interval $[0; \pi/2]$. This adds up to a total of $\sim 2 \times 10^4$ grid points. The numerical minimization is performed using molecular dynamics-type simulated annealing.^{62–64} Our convergence criterion relies on the norm ϵ defined as the maximum of the standard Euclidean vector norm for the difference of the numerical “vector” $\rho(z, \theta = \text{const})$ between two minimization steps, and we take $\epsilon < 10^{-6}$ as the threshold. For low values of the chemical potential μ^* , and hence far away from the coexistence region, $\sim 10^2$ steps were sufficient to obtain convergence. At higher values of μ^* , close to its value at IN coexistence, up to $\sim 10^5$ steps were necessary to obtain convergence.

IV. Results

A. Bulk Properties of Hard Platelets. For the bulk IN transition we obtain from FMT the value of the chemical potential at coexistence, density of the isotropic and the nematic phase, and order parameter in the isotropic and the nematic phase, as $\mu_{\text{coex}}^* = 5.004$, $\rho_I R^3 = 0.419$, $\rho_N R^3 = 0.469$, $S_N = 0.531$, $S_I = 0.045$, respectively. These values differ slightly from those reported in ref 44, where no z -dependence was resolved and hence higher angular resolution with 100 grid points could be used, resulting in⁴⁴ $\rho_I R^3 = 0.418$, $\rho_N R^3 = 0.460$, $S_N = 0.492$, and $S_I = 0$. Both data sets are in good agreement with the simulation results,⁵ which are $\rho_I R^3 = 0.460$, $\rho_N R^3 = 0.498$, and $S_N = 0.45 - 0.55$. Second virial theory gives $\rho_I R^3 = 0.666$, $\rho_N R^3 = 0.849$, and $S_N = 0.79$; hence, it correctly predicts a first-order transition but overestimates both the density jump and the order parameter at coexistence. Figure 2a shows the order parameter S as a function of the scaled bulk density ρR^3 across the IN transition to illustrate these results. In Figure 2b, we plot the equation of state, i.e., the pressure P as a function of ρR^3 . In the isotropic phase within DFT, we use $P(\rho) = -\partial/\partial V(F_{\text{id}}[\rho = \text{const}] + F_{\text{exc}}[\rho = \text{const}])$, and from FMT, we obtain $\beta P(\rho) = \rho + \pi^2 R^3 \rho^2/2 + 2\pi^2 R^6 \rho^3/3$ with $\beta F_{\text{id}}[\rho = \text{const}]/V = \rho(\ln(\rho R^3) - 1)$ and $\beta F_{\text{exc}}[\rho = \text{const}]/V = \pi^2 R^3 \rho^2/2 + \pi^2 R^6 \rho^3/3$. In Onsager theory, the pressure and the excess free energy are given by the same expressions without the contribution of third order in density. In the nematic phase, we insert the equilibrium density distribution into the grand potential functional (2) and use $P = -\bar{\Omega}([\rho], \mu)/V$. For comparison, we have determined the equation of state from isobaric MC simulations using very long runs of up to 10^6 cycles for a system of 500 particles. Figure 2b shows that these simulation results are consistent with those of earlier simulation studies^{4,65,66} and are very well reproduced by the FMT. Onsager theory underestimates the pressure in the isotropic phase and overestimates the pressure in the nematic phase. This is due to the too large coexistence densities leading to a too large density of the coexisting nematic phase. Note also that the slope $dP/d\rho$ is too small in the Onsager treatment.

B. Free Isotropic–Nematic Interface. At bulk IN coexistence, a planar interface that separates the isotropic and nematic phases will be stable. The behavior of such an inhomogeneous system is conveniently analyzed using an orientation-averaged density profile, which gives the density of platelet midpoints at distance z (measured from the position of the Gibbs dividing interface) and is obtained from the full density profile as

$$\rho(z) = \int_0^{\pi/2} d\theta \sin(\theta) \rho(z, \theta) \quad (16)$$

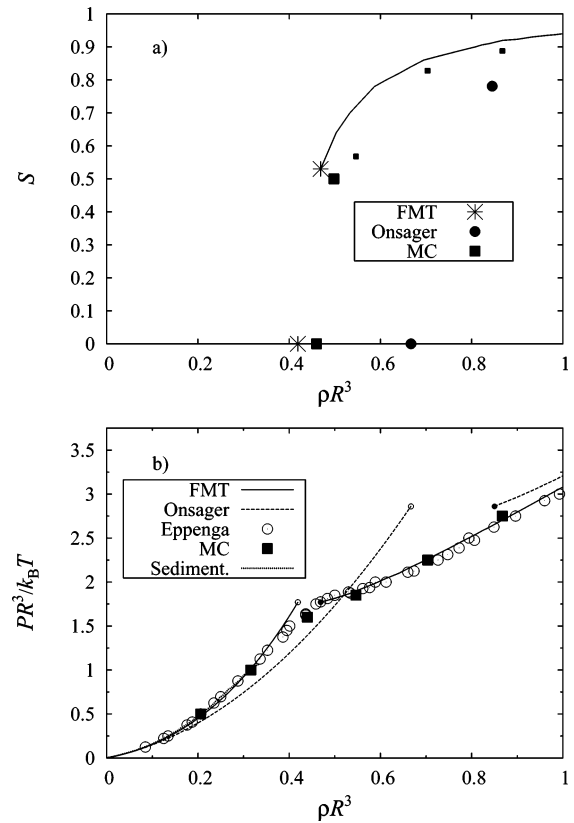


Figure 2. (a) Nematic order parameter S and bulk density ρR^3 at coexistence as obtained from FMT (big stars), MC simulations (squares), and Onsager theory (closed circles). Also shown is S as a function of ρR^3 in the nematic phase from FMT (full line) and MC simulation (small squares). (b) Scaled pressure $PR^3/k_B T$ as a function of the bulk density ρR^3 as obtained from FMT (full line), MC simulations (black squares), and Onsager theory (dashed line). Also shown are the MC simulation results of ref 4 (open circles) and those obtained from sedimentation profiles (dotted line); see ref 66. The small open and closed circles indicate the theoretical results for the isotropic and nematic coexisting phases, respectively.

To assess the degree of local nematic order, we use the nematic order parameter profile, defined as

$$S(z) = [\rho(z)]^{-1} \int_0^{\pi/2} d\theta \sin(\theta) \rho(z, \theta) P_2(\cos \theta) \quad (17)$$

where $P_2(x) = (3x^2 - 1)/2$ is the second Legendre polynomial. (The normalization is such that $S = 0$ indicates isotropic states, while $S = 1$ indicates parallel alignment of particles.)

We first investigate properties of the free IN interface as obtained from FMT. Figure 3a shows the density profile across the interface for perpendicular alignment of the nematic director with the surface, i.e., such that the platelets tend to lie flat against the free IN interface. The preference for homeotropic anchoring was consistently found by experimental investigations⁵⁰ and for the Zwanzig model.⁴³ The interface is smooth and crosses over monotonically between the densities of the coexisting phases, without any signs of oscillations. We have analyzed the asymptotic decay of the density profile into the bulk phases in detail. For monotonic behavior, we expect that for $z \rightarrow -\infty$, i.e., on the nematic side of the interface, $|\rho(z) - \rho_N| \propto \exp(-|z/\xi_N^p|)$, while for $z \rightarrow \infty$, i.e., on the isotropic side, $|\rho(z) - \rho_I| \propto \exp(-|z/\xi_I^p|)$, where ξ_I^p and ξ_N^p are the correlation lengths in the coexisting I and N phases, respectively (the upper index is a reminder of their relationship to $\rho(z)$). We hence plot in the insets of Figure 3a $\ln|\rho(z) - \rho_I|$ on the isotropic side and

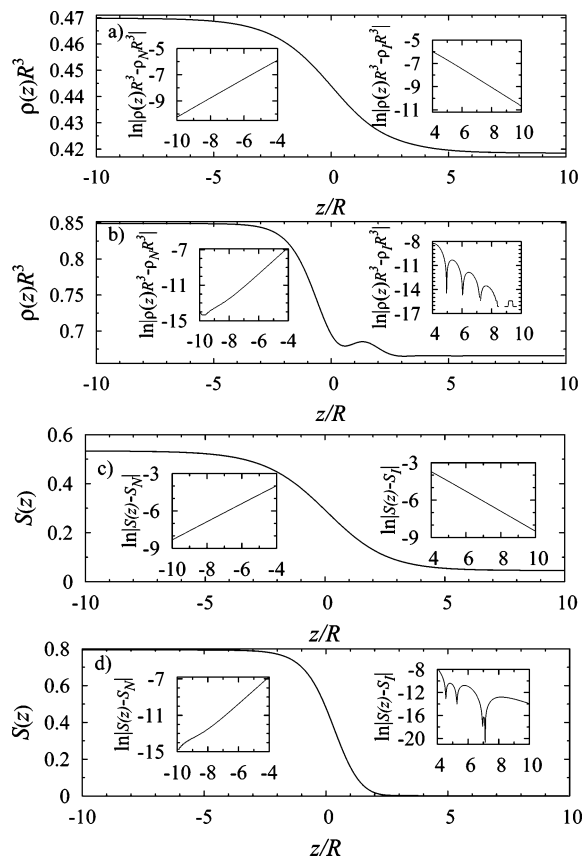


Figure 3. Density profile $\rho(z)R^3$ (parts a and b) and order parameter profile $S(z)$ (parts c and d) across the free IN interface as obtained from FMT (a and c) and Onsager theory (b and d). The insets show $\ln|\rho(z)R^3 - \rho_{IN}R^3|$ and $\ln|S(z) - S_{IN}|$, revealing an asymptotic monotonic exponential decay into the bulk phases in all cases except for the oscillatory decay into the isotropic phase as predicted by the Onsager theory in b and d.

$\ln|\rho(z) - \rho_N|$ on the nematic side of the interface as a function of z . The observed linear dependence confirms the expectation, and from the slopes we obtain $\xi_1^o/R = 1.32$ and $\xi_N^o/R = 1.35$. Corresponding results for $\rho(z)$ from Onsager theory are shown in Figure 3b and will be discussed below. Figure 3c shows the order parameter profile across the IN interface as obtained from FMT. Again, we have analyzed the asymptotic decay of the profile and find that the order parameter decays for $z \rightarrow -\infty$ as $|S(z) - S_N| \propto \exp(-|z/\xi_N^S|)$, where $\xi_N^S/R = 1.33$, and for $z \rightarrow \infty$ as $|S(z) - S_I| \propto \exp(-|z/\xi_1^S|)$ where $\xi_1^S/R = 1.28$; see the inset of Figure 3c. (Note that S_I is nonvanishing only for numerical reasons.) We expect that $\xi_1^o = \xi_1^S$ and $\xi_N^o = \xi_N^S$ and indeed find this to good accuracy to be fulfilled, demonstrating the internal consistency of our calculations.

Results from Onsager theory for the density profile and order parameter profile at the free IN interface are plotted in Figure 3b and d, respectively. Indeed weak oscillations at the *isotropic* side of the free IN interface can be observed. See the insets (left) on the nematic side of Figure 3b and d, where $\rho(z)$ and $S(z)$ are shown, respectively, on a logarithmic scale. At the nematic side of the interface, Onsager theory predicts a monotonic exponential decay, both for the density and the order parameter, with a decay length given by $\xi_N^o/R = \xi_N^S/R \approx (0.67 \pm 0.01)$. This shorter decay length, compared to that from the FMT calculations, is also reflected by the sharper interface and the steeper slopes in the Onsager profiles. We will discuss the relationship of the asymptotic decay at the free IN interface with that at a hard wall in more detail in section IV C.

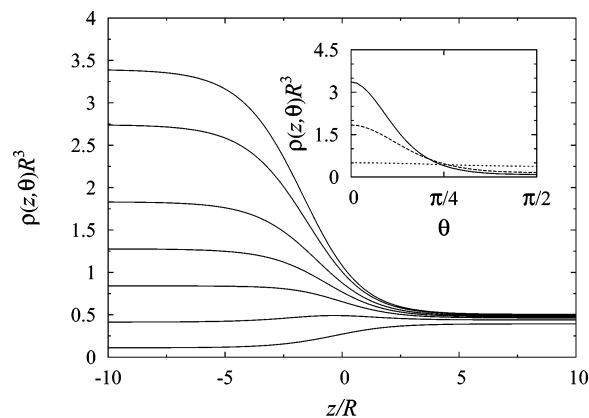


Figure 4. Variation of $\rho(z, \theta)R^3$ with z across the free IN interface for seven different angles, $\theta = 0, 0.2, 0.36, 0.47, 0.58, 0.78,$ and $1.57 = \pi/2$ (from top to bottom) as obtained from FMT. The inset shows $\rho(z, \theta)R^3$ as a function of θ for $z/R = -10, 0,$ and 10 (solid line, dashed line, and dotted line, respectively).

To illustrate the properties of the free IN interface further, we plot in Figure 4 results from FMT for $\rho(z, \theta)$ as a function of z/R for seven different values of θ . We find that for $\theta \rightarrow \pi/2$ the density in the nematic phase is lower than in the isotropic phase, which is due to the ordering in the nematic phase around the nematic director at $\theta = 0$; this causes lower densities around $\theta = \pi/2$. Furthermore, the inset of Figure 4 shows $\rho(z, \theta)$ as a function of θ for three different fixed values of z/R , where $z/R = -10$ is on the nematic side, $z = 0$ is at the Gibbs dividing surface, and $z/R = 10$ is on the isotropic side of the interface. The crossover from an isotropic orientation distribution to one characteristic for the nematic phase is clearly visible.

In the following, we explore the repercussions of the interfacial properties of the free IN interface on the adsorption behavior of platelets at a hard wall.

C. Adsorption of Platelets at a Hard Wall. The hard wall constitutes a basic yet realistic model for a substrate, e.g., a container wall, that a colloidal dispersion is exposed to. Although only represented by a hard core constraint, the hard wall induces coupling of orientation and translation degrees of freedom, because the restriction of available orientations depends on the distance of the particle center to the wall (see eq 1 for the definition of the external potential). Figure 5a shows orientation-averaged density profiles, $\rho(z)R^3$ (as defined in eq 16), obtained from FMT for a range of chemical potentials approaching bulk IN coexistence. For low values of μ^* , and correspondingly low values of the scaled bulk density, ρR^3 , a pronounced “correlation hole” is apparent close to the wall.⁴⁰ This originates from the reduction in available configurations due to overlap of the platelet with the wall. At $z = R$, there is a sharp cusp, followed by weak oscillations for larger distances z . Quite unexpectedly, but consistent with the monotonic decay at the free IN interface, these oscillations disappear upon increasing μ^* . A further shoulder appears very close to the wall, $z \sim 0.5R$, which develops into an independent peak that grows in size and becomes eventually larger than the cusp at $z = R$. A pronounced wetting film grows upon approaching bulk IN coexistence. The film decays from a plateau with a value that is very similar to the density of the coexisting nematic phase smoothly to the value of the isotropic bulk. To demonstrate the similarity between the wetting film at the hard wall and the free IN interface, we superimpose the density profile of the free IN interface onto the profile exhibiting the thickest wetting film in Figure 5a. We show results from Onsager theory for density profiles at the hard wall for a range of different bulk densities

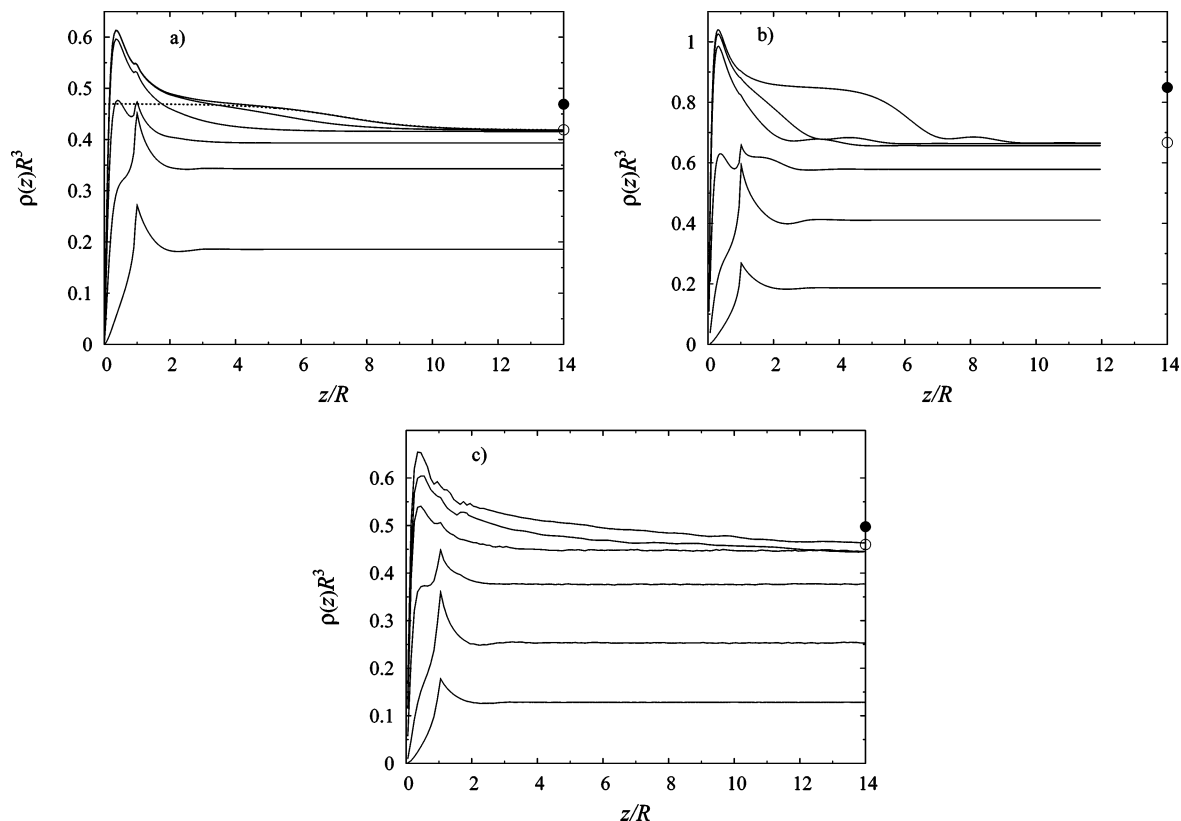


Figure 5. (a) Density profiles from FMT as a function of the distance from the wall, $\rho(z)R^3$, for values of the scaled (bulk) density $\rho R^3 = 0.186, 0.343, 0.393, 0.416, 0.4182, 0.4184$ (from bottom to top). The dotted line is the profile across the free IN interface. Bulk isotropic and nematic coexistence densities are indicated by the open and closed circles. (b) Density profiles from Onsager theory as a function of the distance from the wall, $\rho(z)R^3$, for values of the scaled (bulk) density $\rho R^3 = 0.187, 0.411, 0.579, 0.657, 0.663, 0.665$ (from bottom to top). Bulk isotropic and nematic coexistence densities are indicated by the open and closed circles. (c) Density profiles as a function of the distance from the wall, $\rho(z)R^3$, from MC simulations, for bulk densities $\rho R^3 = 0.125, 0.25, 0.38, 0.45, 0.46, 0.475$ (from bottom to top). Bulk isotropic and nematic coexistence densities are indicated by the open and closed circles.

in Figure 5b. The profiles for small bulk densities are very similar to those obtained from FMT. With increasing density, a nematic wetting layer develops. The behavior close to the wall is very similar to that found in FMT. Also a wetting film develops, but this is much more pronounced compared to the FMT results, consistent with the trend of the differences in coexistence densities obtained from both approaches.

In order to test the theoretical results we have carried out *NVT* MC simulations using very large system sizes with up to $N = 7 \times 10^4$ hard platelets confined between two planar hard walls. As the interfacial tension between the isotropic and nematic phase is very low, we needed large (lateral) wall areas in order to stabilize the nematic film against thermal fluctuations. Moreover, large wall separations were needed to prevent capillary nematization. The density profiles obtained from MC simulations are shown in Figure 5c. Note that the bulk densities chosen are different from those considered in DFT to account for differences in the bulk coexistence densities. The density profiles from MC simulations confirm the existence of a correlation hole close to the wall and the cusp at $z = R$ for low densities. With increasing density, this peak is overshadowed by a growing peak at $z \sim 0.5R$, in agreement with the results from DFT. The growing wetting film is very similar but somewhat more diffuse than that found by FMT. We attribute this to the presence of additional (capillary wave) fluctuations in the simulations that are not captured in DFT.

We next investigate the origin of the maximum at $z \sim 0.5R$ that occurs for high bulk densities; see Figure 5 for results from both DFTs and from simulations. In Figure 6, we have chosen $\rho R^3 = 0.4184$ as an example value and have plotted the wall

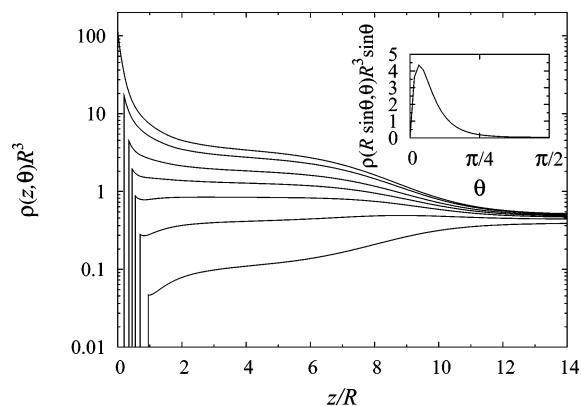


Figure 6. Variation of $\rho(z, \theta)$ with z for seven different angles, $\theta = 0, 0.2, 0.36, 0.47, 0.58, 0.78, 1.57 = \pi/2$ (from top to bottom) as obtained from FMT on a logarithmic vertical axis. The inset shows the contact value $\rho(R \sin \theta, \theta) \sin \theta$ as a function of θ .

density profile $\rho(z, \theta)$ as a function of z for seven different fixed values of the angle θ . We find that the first (contact) peak moves away from the wall for increasing values of θ . This is due to the orientation-dependent hard core repulsion that the wall exerts on the particles; in particular, only platelets with $\theta = 0$ are allowed to lie with their centers directly at the wall, $z = 0$. The inset in Figure 6 shows the wall contact value of the density distribution $\rho(R \sin \theta, \theta) \sin \theta$ as a function of θ ; the spherical volume element is accounted for by the factor $\sin \theta$. We find that—due to the $\sin \theta$ term—the maximum lies *not* at the wall. Together with the fact that the averaged density profile $\rho(z)R^3$

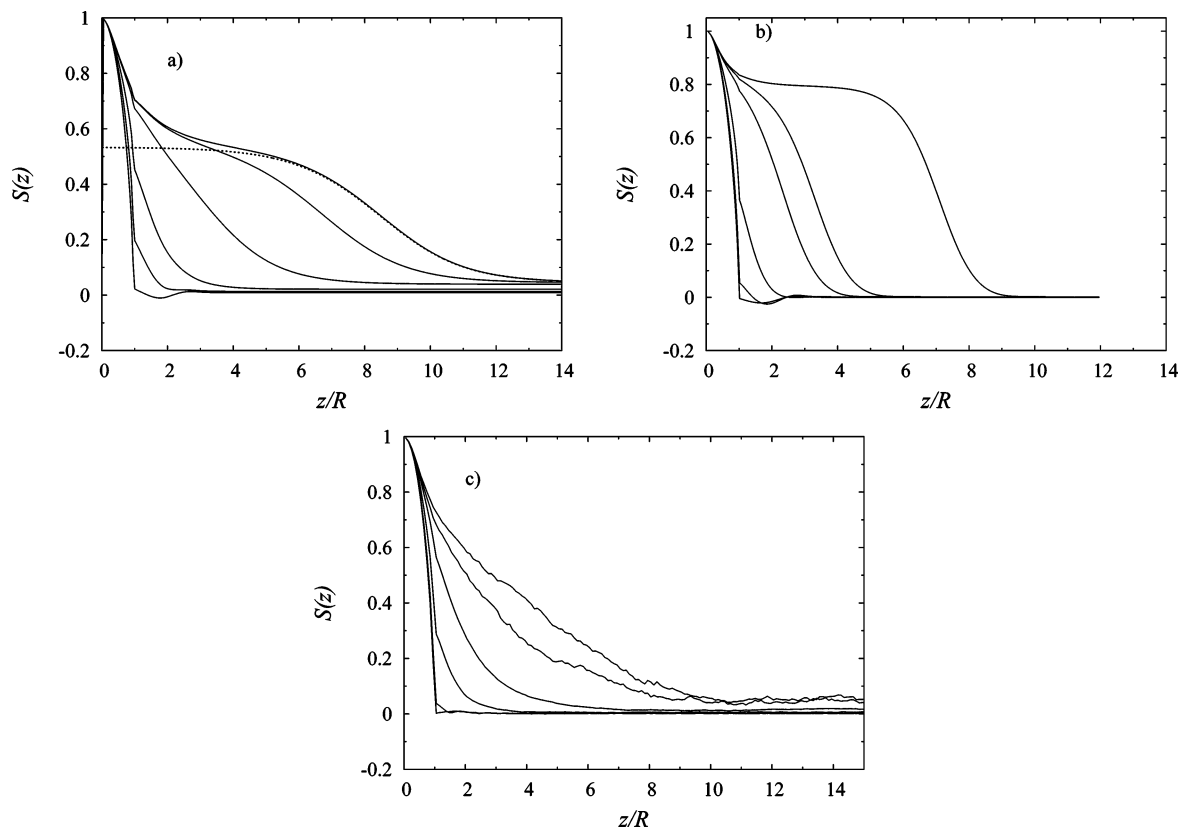


Figure 7. (a) Nematic order parameter profile from FMT, $S(z)$, as a function of the distance from the hard wall for the same values of ρR^3 as in Figure 5a. The dotted line shows $S(z)$ across the free IN interface. (b) Order parameter profiles from Onsager theory, as a function of the distance from the wall. Plotted are results for the same bulk densities as in Figure 5b. (c) Nematic order parameter profile, $S(z)$, from MC simulations as a function of the distance from the hard wall, for the same values of ρR^3 as in Figure 5c.

is defined as an integral over θ (see eq 16), this helps to explain the maximum at $z \sim 0.5R$.

In Figure 7a, we show the order parameter profile $S(z)$ at the hard wall from FMT for the same statepoints as considered in Figure 5a. Upon approaching the wall, the order parameter approaches unity, as platelets with small separation distances from the wall must be well aligned with the wall to avoid overlap. For low bulk densities, there is a minimum of $S(z)$ near $z \sim 2R$. Strikingly, upon increasing the chemical potential, a growing zone of nematic order is found. This confirms that indeed the film of high density possesses nematic order. Figure 7b shows order parameter profiles at the hard wall as obtained from Onsager theory for the same bulk densities as considered in Figure 5b. Again, results from FMT and Onsager are very similar for small densities. A strongly pronounced nematic wetting layer is also found for bulk densities close to IN coexistence. Corresponding results from MC simulations are shown in Figure 7c. Although the MC data contain some statistical noise and the minimum in $S(z)$ is not found in the simulations, the overall agreement to the results from FMT is striking.

Figure 8 shows the asymptotic behavior of $\rho(z)$ for large distances from the wall for three different (bulk) densities as obtained from FMT (a), Onsager (b), and MC (c) simulations. To scrutinize the behavior, we plot $\ln|\rho(z)R^3 - \rho R^3|$, which allows the observation of oscillations with small amplitude more easily than a linear plot does. Note that zeros of $\rho(z) - \rho$ correspond to (negative) poles of $\ln|\rho(z)R^3 - \rho R^3|$. For numerical reasons, the curves in Figure 8 display only a finite negative minimum value; these (relatively) deep local minima correspond to the zeros of $\rho(z)$. While the first minimum is due to the initial increase of the density from the wall, the subsequent

minima stem from oscillations of the density profile that extend into the bulk. Hence, the monotonic decay of the upper profiles obtained from FMT in Figure 8a indicates that the oscillations disappear upon increasing density. This finding is supported by the MC simulations, although in Figure 8c for $z/R > 3.5$ the statistical errors are considerable. In contrast to this scenario, Onsager theory predicts oscillations over the full range of densities in the isotropic phase; see Figure 8b. The oscillations move away from the wall with increasing density, but do not disappear. In Figure 9a and b, we show the results for the order parameter $S(z)$ obtained from FMT (corresponding to Figure 8a) and Onsager theory (corresponding to Figure 8b), respectively. Again, the FMT results indicate a crossover from oscillatory to monotonic decay upon increasing density, while Onsager theory predicts oscillatory decay over the full range of densities in the isotropic phase. Crossover from monotonic to oscillatory decay of density profiles at the free interface between demixed nematic phases was found in mixtures of large and small Zwanzig platelets,⁴³ and the authors conclude that a Fisher–Widom line separating these different regimes must exist in this system. Here, however, we find such structural crossover in the isotropic phase.

The nature of the wetting scenario can be analyzed in more detail by considering the adsorption, either obtained from $\rho(z)$ or from $S(z)$, via

$$\Gamma_\rho = \int_0^\infty dz [\rho(z) - \rho(\infty)] \quad (18)$$

$$\Gamma_S = \int_0^\infty dz [S(z) - S(\infty)] \quad (19)$$

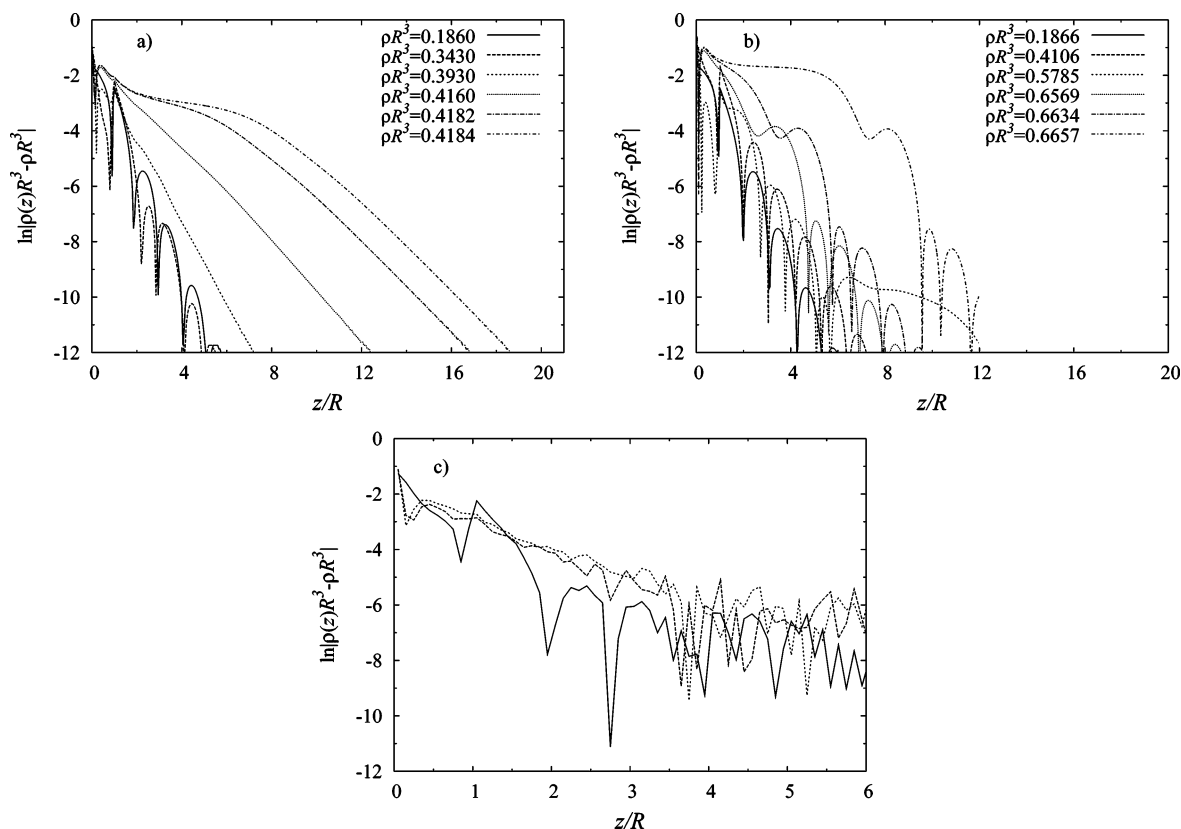


Figure 8. (a) Variation of $\ln|\rho(z)R^3 - \rho R^3|$ with z/R for the same values of (bulk) density as in Figure 5a, as obtained from FMT. (b) Same as part a but from Onsager theory for the (bulk) densities of Figure 5b. (c) Same as a and b but as obtained from MC simulations for $\rho R^3 = 0.306, 0.444,$ and 0.459 (from bottom to top).

In Figure 10a, we have plotted Γ_ρ as obtained from FMT as a function of the scaled density ρR^3 in the isotropic and nematic phase. The adsorption is negative for low densities and has a minimum at $\rho R^3 \approx 0.2$. For $\rho R^3 > 0.3$, we find positive values of Γ_ρ , and eventually, a sharp increase as ρ approaches its value in the coexistent isotropic phase. This hints at complete wetting of the wall by the nematic phase. In the nematic phase, the adsorption decreases monotonically as a function of ρR^3 . This can be explained with increasing nematic ordering in the bulk and hence a loss of structure close to the wall. The film thickness, defined via $d_\rho = \Gamma_\rho/(\rho_N - \rho_I)$ and $d_S = \Gamma_S/(S_N - S_I)$, is shown in the inset of Figure 10a as a function of $-\ln(\Delta\mu^*)$, with $\Delta\mu^* = \mu_{\text{coex}}^* - \mu^*$. From the fact that we find a linear dependence in this representation, we can conclude that the nematic phase wets the wall completely, i.e., that the film thickness diverges as bulk coexistence is approached as⁶⁷

$$d_\rho = \xi_N^\rho \ln(\Delta\mu^*) + \text{const} \quad (20)$$

$$d_S = \xi_N^S \ln(\Delta\mu^*) + \text{const} \quad (21)$$

which is indeed appropriate for complete wetting in the present case of short-ranged interparticle forces. Complete wetting of a hard wall by the nematic phase has also been found for the Zwanzig model for platelets with restricted orientations.⁴² We find $\xi_N^\rho/R = 1.32$ and $\xi_N^S/R = 1.22$. While the agreement with the data from the decay of the free IN interface for ξ_N^ρ is very good, the above given value for ξ_N^S is slightly smaller than that found at the free IN interface, which we attribute to the larger sensitivity of the order parameter S to numerical uncertainties.

In addition, we consider Young's equation for the contact angle ϑ at which the free IN interface hits the wall,

$$\cos \vartheta = \frac{\gamma_{\text{WI}} - \gamma_{\text{WN}}}{\gamma_{\text{IN}}} \quad (22)$$

where γ_{WN} , γ_{WI} , and γ_{IN} are the interfacial tensions between the wall and the nematic phase, between the wall and the isotropic phase, and between the isotropic and the nematic phase, respectively. Results for the tensions are obtained from the general definition of the interfacial tension,

$$\gamma = (\Omega_{\text{inh}} + pV)/A \quad (23)$$

where Ω_{inh} is the grand potential of the inhomogeneous system exhibiting the interface, p is the bulk pressure, V is the system volume, and A is the interface area. Within DFT, Ω_{inh} is obtained from inserting the equilibrium result for $\rho(z, \theta)$ into eq 2, i.e., $\Omega_{\text{inh}} = \Omega[\rho(z, \theta)]$. Within FMT, we find $\gamma_{\text{WN}}R^2/k_B T = 0.3327$, $\gamma_{\text{WI}}R^2/k_B T = 0.3391$, and $\gamma_{\text{IN}}R^2/k_B T = 0.006656$ (see section IV B) from eq 23, which yields $\cos \vartheta \approx 0.96$. Because γ_{IN} is obtained from two numerically similar quantities via (23), the resulting value has a relatively large numerical uncertainty. Keeping this in mind when using γ_{IN} in (22), the result $\cos \vartheta \approx 0.96$ is consistent with $\vartheta = 0$ as appropriate for complete wetting. The corresponding values from Onsager theory are given by $\gamma_{\text{WI}}R^2/k_B T = 0.4387$, $\gamma_{\text{WN}}R^2/k_B T = 0.3878$, $\gamma_{\text{IN}}R^2/k_B T = 0.0508$, such that $\cos \vartheta = 1.003$, again within the numerical accuracy consistent with $\vartheta = 0$ and hence complete wetting.

In the simulations we use thermodynamic integration to determine the free energy difference of a bulk system and a system with a wall. We approximate the hard wall by a finite

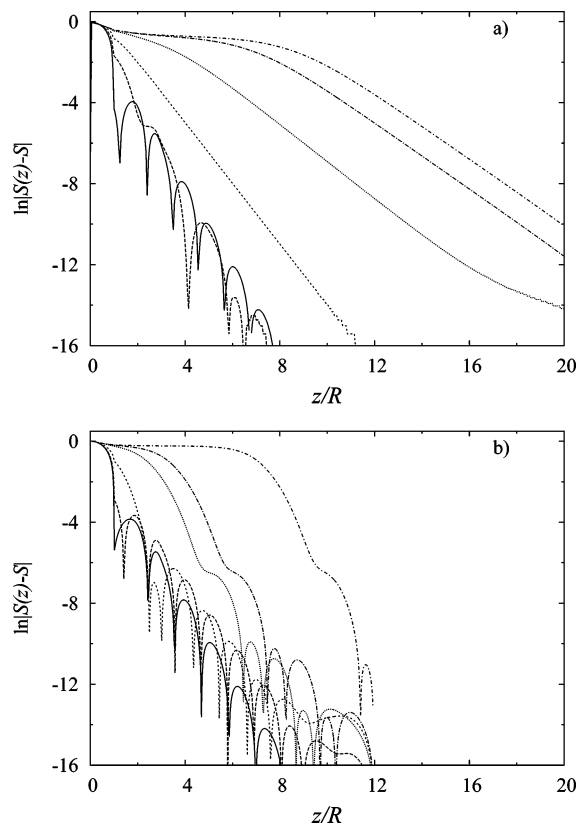


Figure 9. (a) Variation of $\ln|S(z) - S|$ with z/R from FMT for the same values of ρR^3 as in Figure 8a. (b) Variation of $\ln|S(z) - S|$ with z/R from Onsager theory for the same values of ρR^3 as in Figure 8b.

barrier, such that a zero barrier height corresponds to a bulk system and an infinite barrier height to a system with a hard wall.^{68,69} This yields the wall tensions γ_{WI} and γ_{WN} and we obtain γ_{IN} via (22) assuming complete wetting, $\vartheta = 0$. We find $\gamma_{IN} R^2 / k_B T = 0.015$ from MC simulations.

In Figure 10b, we have plotted the wall interfacial tension $\gamma R^2 / k_B T$ as a function of the (bulk) density far away from the wall $\rho = \rho(\infty)$. At low densities, $\rho R^3 \lesssim 0.3$, we find very good agreement between results from both DFTs and the simulations, as well as with the tension obtained from scaled-particle theory (SPT),⁷⁰ given by

$$\gamma / k_B T = \pi \rho R / 4 + \pi \rho^2 R^4 / 2 \quad (24)$$

The SPT result fails, however, to reproduce the maximum of γ that occurs below bulk coexistence. There is very good agreement between the location of this maximum ($\rho R^3 \approx 0.4$) in FMT and MC, whereas Onsager theory locates it far off at $\rho R^3 \approx 0.6$. The nonmonotonic behavior of γ is accompanied by the growth of the nematic wetting layer, leading to a reduction of the interfacial tension. In the nematic phase, γ decreases as a function of ρR^3 , which we can trace back to the increasing nematic order in the bulk. The decay predicted by FMT is stronger than that found in the simulations. Although the Onsager functional overestimates the behavior in the coexistence region significantly, it gives a qualitatively correct picture.

V. Conclusions

In conclusion, we have used two different versions of density functional theory as well as MC computer simulations to investigate bulk and interfacial properties of a model colloidal dispersion of hard circular platelets with vanishing thickness.

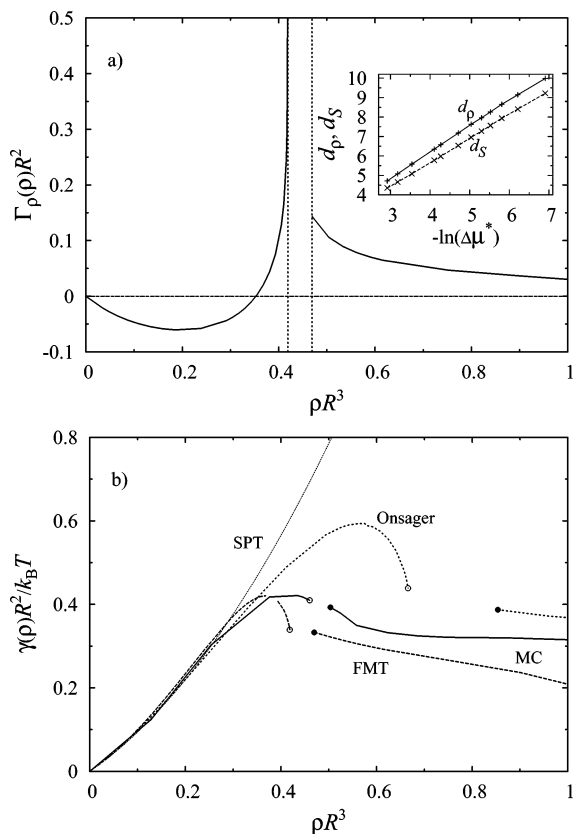


Figure 10. (a) Adsorption $\Gamma_\rho R^2$ as a function of the density ρR^3 , as obtained from FMT. The vertical lines indicate the isotropic and nematic coexistence density. The divergence of Γ_ρ is a signature of complete wetting of the wall. The inset shows FMT results for the thickness d_ρ (upper line) and d_S (lower line) of the nematic wetting film, as defined in the main text, as a function of $-\ln(\Delta\mu^*)$. (b) Interface tension γ at a hard wall as a function of the scaled bulk density ρR^3 , as obtained from FMT (long dashed line), Onsager theory (short dashed line), scaled particle theory (dotted line), and MC simulations (full line). The open and filled circles represent the values at bulk isotropic and nematic coexistence statepoints, respectively, as obtained from FMT, simulations, and Onsager theory.

The system displays a density-driven, weak first-order IN transition with a small density jump at coexistence ($\sim 8\%$) and an unusually low-order parameter in the coexisting nematic phase ($S \sim 0.5$). Results for the equation of state in both the isotropic and in the nematic phase and the location of the bulk IN transition obtained from the FMT version of DFT agree well with those from MC simulations. For low densities, the FMT version reduces to the Onsager (second virial) version of DFT, and we can verify corresponding agreement of results from both approaches for low densities. For higher densities, the Onsager theory gives only a qualitatively correct picture: It predicts the IN transition correctly to be of first order, but already at densities $\rho R^3 \sim 0.2$, well below the phase transition, deviations of the pressure to that obtained from simulations become apparent, indicating that higher than second-order virial coefficients become important. As the Onsager theory misses such contributions, considerably too high densities are needed to induce sufficiently strong contributions to the free energy that drive the system into a nematic state. In turn, the nematic phase at coexistence has a profoundly too high density and too high nematic order parameter, according to Onsager theory.

When adsorbed against a hard wall, we find in both versions of DFT as well as in the simulations complete wetting of the wall by the nematic phase upon increasing the bulk density toward the density of the isotropic phase at coexistence. Within

FMT, we conclude the occurrence of complete wetting both from an analysis of the divergence of the adsorption due to the formation of the nematic wetting film and from Young's equation, which yields a vanishing contact angle within the numerical accuracy. The results for the density profiles at a hard wall obtained from FMT compare favorably to those from MC simulations. Both the detailed variation of the density with distance within a few particle radii of distance from the wall as well as the growth of a wetting film of high density upon approaching the bulk isotropic coexistence density are reproduced by the theory. The most prominent difference is that the decay of the profiles to the bulk value is somewhat more diffuse in the simulations. We attribute this to the influence of capillary fluctuations of the free interface,^{71,72} which are not accounted for in the DFT. Investigating the wall isotropic interfacial tension, we have found that the FMT results are in close agreement with the simulation data. Onsager theory overestimates the value of the wall interfacial tension at high densities; again at low densities $\rho R^3 \lesssim 0.3$, the results compare well to those from the other approaches.

Our investigation of the precise form of the asymptotic decay of the density profile at large distances z from a planar interface remains somewhat inconclusive. In the nematic phase, we have considered in detail the case where the nematic director at large distances from the interface is aligned with the interface normal (i.e., the z -direction). We have established, consistently within both theories, that the decay is monotonic in this case. As the platelet diameter D is the only relevant length scale in the system, we would expect possible oscillations to possess wavelengths comparable to D and hence to originate from packing effects of particles that lie *perpendicular* to the z -direction. Clearly, such configurations are strongly suppressed in the nematic phase, and indeed, no oscillatory behavior is observed in this geometry. The most probable particle configurations parallel to the director, however, are not expected to lead to oscillations, as there is no apparent intrinsic length scale for platelets with vanishing thickness that could lead to such oscillations. Our results rule out the presence of oscillations with smaller wavelength than D . What remains to be investigated, however, is the decay for different inclinations of the nematic director (far away from the interface) and the surface normal, in particular the case where both are parallel.

We have established that in the isotropic phase (where the above dependence on relative orientations is absent) the asymptotic decay far from the planar hard wall is indeed oscillatory for low densities. Both DFTs predict that this type of decay persists over most of the range of densities in the isotropic phase. While the simulation results do not invalidate this scenario, the considerable statistical uncertainties prohibit obtaining supporting evidence as well. One prominent difference between the Onsager and FMT results is that the latter clearly show a crossover from damped oscillatory to monotonic exponential decay upon increasing density, at a value close to but definitely below the isotropic coexistence density. As we expect the asymptotic decay to be universal, this is consistent with the fact that we have found monotonic decay at the isotropic side of the *free* IN interface within FMT, whereas Onsager theory gives rise to damped oscillatory decay. Whether the observed crossover in the isotropic phase, and hence an unusual disappearance of a signature of packing effects upon increasing density, indeed reflects a crossover in the type of structural correlations, or is rather an artifact of the DFT approximation or its numerical discretization, remains to be seen. Clearly, relating the asymptotic decay of the one-body density

profile to that of the asymptotic decay of bulk pair correlation functions could shed further light on this topic.⁷³

Possible future research could be aimed at capillary effects inside planar pores,⁴² capillary waves at the free IN interface,^{71,72} or the influence of an external magnetic or gravitational field on the behavior of the dispersion. A further interesting point of investigation is the effect of the softness of the wall-platelet potential on the adsorption properties.⁷⁴

Acknowledgment. We thank D. van der Beek, P. van der Schoot, T. Schilling, R. L. C. Vink, and, in particular, H. N. W. Lekkerkerker for very fruitful discussions. This work is supported by the SFB-TR6 "Colloidal dispersions in external fields" of the German Science Foundation (Deutsche Forschungsgemeinschaft) under project section D3. This work is part of the research programme of the "Stichting voor Fundamenteel Onderzoek der Materie (FOM)", which is financially supported by the "Nederlandse Organisatie voor Wetenschappelijk Onderzoek (NWO)".

References and Notes

- (1) Zocher, H. Z. *Anorg. Chem.* **1925**, *147*, 91.
- (2) Bawden, F. C.; Pirie, N. W.; Bernal, J. D.; Fankuchen, I. *Nature* **1936**, *138*, 1051.
- (3) Onsager, L. *Ann. N.Y. Acad. Sci.* **1949**, *51*, 627.
- (4) Frenkel, D.; Eppenga, R. *Phys. Rev. Lett.* **1982**, *49*, 1089.
- (5) Bates, M.; Frenkel, D. *Phys. Rev. E* **1998**, *57*, 4824.
- (6) Rosenfeldt, S.; Karpuk, E.; Lehmann, M.; Meier, H.; Lindner, P.; Harnau, L.; Ballauf, M. *ChemPhysChem* **2006**, *7*, 2097.
- (7) van der Kooij, F. M.; Kassapidou, K.; Lekkerkerker, H. N. W. *J. Phys. Chem. B* **1998**, *102*, 7829.
- (8) van der Kooij, F. M.; Kassapidou, K.; Lekkerkerker, H. N. W. *Nature* **2000**, *106*, 868.
- (9) van der Beek, D.; Petukhov, A. V.; Oversteegen, S. M.; Vroege, G. J.; Lekkerkerker, H. N. W. *Eur. Phys. J. E* **2005**, *16*, 253.
- (10) van der Beek, D.; Lekkerkerker, H. N. W. *Europhys. Lett.* **2003**, *61*, 702.
- (11) van der Beek, D.; Lekkerkerker, H. N. W. *Langmuir* **2004**, *20*, 8582.
- (12) Wijnhoven, J. E. G. J.; van 't Zand, D. D.; van der Beek, D.; Lekkerkerker, H. N. W. *Langmuir* **2005**, *21*, 10422.
- (13) van der Beek, D.; Schilling, T.; Lekkerkerker, H. N. W. *J. Chem. Phys.* **2004**, *121*, 5423.
- (14) van der Beek, D.; Petukhov, A. V.; Davidson, P.; Ferre, J.; Jamet, J. P.; Wensink, H. H.; Vroege, G. J.; Bras, W.; Lekkerkerker, H. N. W. *Phys. Rev. E* **2006**, *73*, 041402.
- (15) Zhang, Z. X.; van Duijneveldt, J. S. *J. Chem. Phys.* **2006**, *124*, 154910.
- (16) Pizzey, C.; van Duijneveldt, J. S.; Klein, S. *Mol. Cryst. Liq. Cryst.* **2004**, *409*, 51.
- (17) Zhang, S. D.; Reynolds, P. A.; van Duijneveldt, J. S. *J. Chem. Phys.* **2002**, *117*, 9947.
- (18) Zhang, S. D.; Reynolds, P. A.; van Duijneveldt, J. S. *Mol. Phys.* **2002**, *100*, 3041.
- (19) Wensink, H. H.; Lekkerkerker, H. N. W. *Europhys. Lett.* **2004**, *66*, 125.
- (20) Wensink, H. H.; Vroege, G. J.; Lekkerkerker, H. N. W. *J. Phys. Chem. B* **2001**, *105*, 10610.
- (21) Harnau, L.; Costa, D.; Hansen, J. P. *Europhys. Lett.* **2001**, *53*, 729.
- (22) Oversteegen, S. M.; Lekkerkerker, H. N. W. *J. Chem. Phys.* **2004**, *120*, 2470.
- (23) Bier, M.; Harnau, L.; Dietrich, S. *J. Chem. Phys.* **2005**, *123*, 114906.
- (24) Martinez-Raton, Y.; Cuesta, J. A. *Phys. Rev. Lett.* **2002**, *89*, 185701.
- (25) Dijkstra, M.; van Roij, R. *J. Phys.: Condens. Matter* **2005**, *17*, S3507.
- (26) Poniewierski, A. *Phys. Rev. E* **1993**, *47*, 3396.
- (27) van Roij, R.; Dijkstra, M.; Evans, R. *Europhys. Lett.* **2000**, *49*, 350.
- (28) van Roij, R.; Dijkstra, M.; Evans, R. *J. Chem. Phys.* **2000**, *113*, 7689.
- (29) Dijkstra, M.; van Roij, R.; Evans, R. *Phys. Rev. E* **2001**, *63*, 051703.
- (30) Schmidt, M.; Löwen, H.; Brader, J. M.; Evans, R. *J. Phys.: Condens. Matter* **2002**, *14*, 9353.
- (31) Roth, R.; Brader, J. M.; Schmidt, M. *Europhys. Lett.* **2003**, *63*, 549.
- (32) Brader, J. M.; Evans, R.; Schmidt, M. *Mol. Phys.* **2003**, *101*, 3349.

- (33) Evans, R.; Brader, J. M.; Roth, R.; Dijkstra, M.; Schmidt, M.; Löwen, H. *Philos. Trans. R. Soc. A* **2001**, *359*, 961.
- (34) Dijkstra, M.; van Roij, R. *Phys. Rev. Lett.* **2002**, *89*, 208303.
- (35) Dijkstra, M.; van Roij, R.; Roth, R.; Fortini, A. *Phys. Rev. E* **2006**, *73*, 041404.
- (36) Bryk, P. *J. Chem. Phys.* **2005**, *123*, 234907.
- (37) Bryk, P. *J. Chem. Phys.* **2006**, *125*, 204709.
- (38) Dijkstra, M. *Phys. Rev. Lett.* **2004**, *93*, 108303.
- (39) Roth, R.; van Roij, R.; Andrienko, D.; Mecke, K. R.; Dietrich, S. *Phys. Rev. Lett.* **2002**, *89*, 088301.
- (40) Harnau, L.; Dietrich, S. *Phys. Rev. E* **2002**, *65*, 021505.
- (41) Harnau, L.; Rowan, D.; Hansen, J.-P. *J. Chem. Phys.* **2002**, *117*, 11359.
- (42) Harnau, L.; Dietrich, S. *Phys. Rev. E* **2002**, *66*, 051702.
- (43) Bier, M.; Harnau, L.; Dietrich, S. *Phys. Rev. E* **2004**, *69*, 021506.
- (44) Esztermann, A.; Reich, H.; Schmidt, M. *Phys. Rev. E* **2006**, *73*, 011409.
- (45) Fisher, M. E.; Widom, B. *J. Chem. Phys.* **1969**, *50*, 3756.
- (46) Evans, R.; Henderson, J. R.; Hoyle, D. C.; Parry, A. O.; Sabeur, Z. A. *Mol. Phys.* **1993**, *80*, 755.
- (47) Evans, R.; de Carvalho, R. J. F. L.; Henderson, J. R.; Hoyle, D. C. *J. Chem. Phys.* **1994**, *100*, 591.
- (48) Savenko, S. V.; Dijkstra, M. *Phys. Rev. E* **2005**, *72*, 021202.
- (49) Grodon, C.; Dijkstra, M.; Evans, R.; Roth, R. *Mol. Phys.* **2005**, *103*, 3009.
- (50) van der Beek, D.; Reich, H.; van der Schoot, P.; Dijkstra, M.; Schilling, T.; Vink, R.; Schmidt, M.; van Roij, R.; Lekkerkerker, H. N. W. *Phys. Rev. Lett.* **2006**, *97*, 087801.
- (51) Evans, R. Density Functionals in the Theory of Nonuniform Fluids. In *Fundamentals of Inhomogeneous Fluids*; Henderson, D., Ed.; Dekker: New York, 1992.
- (52) Martinez-Raton, Y.; Cuesta, J. A. *J. Chem. Phys.* **1999**, *111*, 317.
- (53) Martinez-Raton, Y.; Cuesta, J. A. *J. Chem. Phys.* **2003**, *118*, 10164.
- (54) Martinez-Raton, Y. *Phys. Rev. E* **2004**, *69*, 061712.
- (55) Martinez-Raton, Y.; Velasco, E.; Mederos, L. *J. Chem. Phys.* **2006**, *125*, 014501.
- (56) Cinacchi, G.; Schmid, F. *J. Phys.: Condens. Matter* **2002**, *14*, 12223.
- (57) Rosenfeld, Y. *Phys. Rev. Lett.* **1989**, *63*, 980.
- (58) Rosenfeld, Y. *Phys. Rev. E* **1994**, *50*, R3318.
- (59) Rosenfeld, Y. *Mol. Phys.* **1995**, *86*, 637.
- (60) Tarazona, P.; Rosenfeld, Y. *Phys. Rev. E* **1997**, *55*, R4873.
- (61) Cuesta, J. A.; Martinez-Raton, Y.; Tarazona, P. *J. Phys.: Condens. Matter* **2002**, *14*, 11965.
- (62) Ohnesorge, R. Dichtestruktur und Schmelzen von Kristallen und ihren Oberflächen. PHD thesis, Ludwig-Maximilians-Universität—München, München, 1994.
- (63) Ohnesorge, R.; Löwen, H.; Wagner, H. *Europhys. Lett.* **1993**, *22*, 245.
- (64) Ohnesorge, R.; Löwen, H.; Wagner, H. *Phys. Rev. E* **1994**, *50*, 4801.
- (65) Eppenga, R.; Frenkel, D. *Mol. Phys.* **1984**, *2*, 1303.
- (66) Dijkstra, M.; Hansen, J. P.; Madden, P. A. *Phys. Rev. E* **1997**, *55*, 3044.
- (67) Schick, M. In *Liquids at Interfaces*; Charvolin, J., Ed.; Elsevier: Amsterdam, 1990.
- (68) Heni, M.; Löwen, H. *Phys. Rev. E* **1999**, *60*, 7057.
- (69) Fortini, A.; Dijkstra, M.; Schmidt, M.; Wessels, P. P. F. *Phys. Rev. E* **2005**, *71*, 051403.
- (70) See, e.g., Oversteegen, S. M.; Roth, R. *J. Chem. Phys.* **2005**, *122*, 214502.
- (71) Akino, N.; Schmid, F.; Allen, M. P. *Phys. Rev. E* **2001**, *63*, 041706.
- (72) Wolfsheimer, S.; Tanase, C.; Shundyak, K.; van Roij, R.; Schilling, T. *Phys. Rev. E* **2006**, *73*, 061703.
- (73) Cheung, D. L.; Allen, M. P. private communication.
- (74) Shundyak, K.; van Roij, R. *Europhys. Lett.* **2006**, *74*, 1039.